MONOLITHIC, PHOTOCONDUCTIVE ULTRA-WIDEBAND RF DEVICE

A. Kim, L. Di Domenico, R. Youmans, A. Balekdjian, and M. Weiner

U.S. Army Research Laboratory, Electronics & Power Sources
Directorate Fort Monmouth, NJ 07703-5601

L. Jasper

U.S. Army Research Laboratory, Weapon Technology Directorate
Adelphi, MD 20783-1197

Abstract

A new monolithic, photoconductive ultra-wideband RF radiating device has been successfully demonstrated. The new device integrates the functions of energy storage, switch, and antenna onto a single semi-insulating(SI)-GaAs wafer substrate, so that the electrostatic energy stored in the device directly converts into ultra-wideband RF radiation. Pulse biasing the device to +2kV and -2kV, and subsequently triggering the device resulted in peak power intensities as high as 14.8 watt/cm at a distance of 40 cm.

1. Introduction

Recently there has been much research activity in ultra-wideband technology. The enormous interest in this technology stems from its potential applications in the fields of impulse radar, impulse communication, and electronic countermeasures. Sub-nanosecond, high peak power impulses are routinely generated using spark gap [1], ferrite pulse sharpening techniques [2], photoconductive semiconductor switches [3].

Typically, the most widely used antenna is a horn antenna. For extremely high frequency applications, the size of antenna maybe made small. However, to obtain hundreds of megahertz frequency, the size of the antenna becomes very large. Since the impulse has a frequency spectrum covering from near DC to several gigahertz, a small antenna for the ultra-wideband radiation will seriously filter out the low frequency components so that the radiation efficiency will be substantially deteriorated.

This paper introduces a new impulse transmitter for generating ultra-wideband RF radiation based on the equiangular spiral antenna. Typically the spiral plate antenna is composed of the two conducting arms and maintains a system balance. Rather than simply feeding the antenna at the center, the energy storaged in the electrodes is converted into the RF pulse. In this structure the functions of the impulse generation and the radiation are combined into a single semi-insulating GaAs substrate.

2. Monolithic, photoconductive Ultra-wideband Transmitter

Monolithic ultra-wideband transmitters were fabricated using a 5 mm thick SI-GaAs wafer. Two different types of the transmitter were obtained by creating the switch region either at the center of the device or at the edge of the spiral arms. In one device the switching action was produced at the center gap between electrodes (Fig. 1). In the second configuration, outer electrodes were added, situated near the periphery of the spirals. The switching was implemented simultaneously in the gap region (2 mm wide) between the spirals and the outer electrodes (Fig. 2). Further, the outer electrode areas of the second transmitter were reduced by a 2 X factor, thus decreasing the capacitance of the energy storage medium. The center gap was not illuminated in the second device. In each device the bottom electrode (Fig. 3) consisted of an outer ring. Thus only the outer regions of the spirals were capacitively coupled to the bottom ring electrode.

CH3277-1/93/0000-1221$01.00 © 1993 IEEE

2. Experimental Results and Discussion

The experimental set-up consisted of a mode-locked Nd:YAG laser, fiber optic bundle, D-dot sensor, charging pulser, and fast oscilloscope. The D-dot sensor (EG&G ACD-4C(R)) was used to measure the radiated waveform from the device. An SCR-transformer pulser was used to pulse charge the two identical capacitors of the monolithic, photoconductive ultra-wideband transmitter with $+V_o$ and $-V_o$, respectively. The measurement sequence consisted of first charging the capacitor with pulse bias voltage, then optically triggering the device, and finally measuring the radiated wave. Upon completion of the charging process the optical pulses from a mode-locked Nd:YAG laser were used to trigger the device. The radiated signal is first monitored by the D-dot sensor, passed through the 2 X attenuator, and then delivered to a Tektronix SCD 5000 oscilloscope.

Radiation waveform from the first device configuration (Fig. 1) is shown in Fig. 4. For this device configuration, the spiral electrodes were pulse biased to +3 kV and -3 kV, respectively, and the center gap was illuminated with a 75 ps wide, optical pulse from a mode-locked Nd:YAG laser. The radiation waveform (Fig. 4) was obtained from the D-dot sensor, located 25 cm away from this device. The radiation waveform from the second device configuration (Fig. 2) is shown in Fig. 5. The radiation measurement for the second device configuration (Fig. 2) was conducted by pulse biasing the device up to +2.0 kV and -2.0 kV, respectively. In this measurement, the D-dot sensor was located 40 cm away from the device.

Three important parameters were obtained: 1) peak to peak output voltage, 2) the RF period, and 3) the total oscillating time. The peak voltage, using a D-dot sensor, was 10 V for the first device, and 30 V in the case of the second device. The typical pulsewidth in both cases was about 1 ns, and the total oscillating times were about 20 ns. No attempt was made to minimize the ringing times.

The radiated power density for the antenna in the free space can be expressed as following:

$$P = E^2/(2 \times 377) \ (w/m^2) \qquad (1)$$

where E is the electric field strength (V/m) and the 377 is the resistance of the free space. The output voltage of the D-dot sensor is expressed as following:

$$V_o = RA_{eq}dD/dt \ (V) \qquad (2)$$

where V_o is the sensor output (in volt), R is the sensor characteristic load impedance (in ohm), A_{eq} is the sensor equivalent area (in m^2), and D is the magnitude of electric displacement (in Coulomb/m^2). The peak power intensities were calculated using Eqs.(1) and (2). The estimated peak power intensities from these devices are 0.38 watt/cm and 14.8 watt/cm, respectively. The superior conversion efficiency of the second device is evident.

There are many possible mechanisms (such as switch risetime, mode of operation, physical dimensions of the energy storage medium, etc.) affecting the RF conversion efficiency. However, the switch risetime and the physical dimensions of the energy storage medium are two most dominant factors. The experimental results obtained with laser diodes (pulse risetime of 4 ns), for example, indicated that the slow switch risetime significantly reduces the amplitude of the radiated RF signal.

Also, the smaller gap spacing of the second device (2 mm), compared to the larger gap (5 mm) of the first device, usually implies a faster switch risetime. The faster switching will enhance the radiation efficiency.

Another important parameter is energy feed mechanism. Depending on the feed configuration, the fundamental antenna time constant (roughly equivalent to the two way wave transit time) can be significantly different. In the case of the first device, the time constant of the pulse biased emery in the annular region may be longer than the fundamental antenna time constant. Analytic

efforts are under way to understand the marked difference in the power intensity between the two designs.

4. Conclusion

A monolithic, photoconductive ultra-wideband impulse transmitter has been successfully demonstrated. The transmitter combines the functions of energy storage, switching, and radiation. Power density was shown to depend significantly on the device configurations. By optimizing the device design, further radiation efficiency enhancement is foreseen.

REFERENCES

[1] L. F. Rinehart, and M. T. Buttram, "Sub-nanosecond Breakdown in Transformer Oil," Proceedings of the Twentieth IEEE Power Modulator Symposium, 1992, pp. 104-106.

[2] D. Birx, , and J. R. Fishback, "High Power, 10 kHz Repetition Rate Ultra- wideband Source Development at the U.S. Army's Missile Command," 1992 IEEE MTT-s International Microwave Symposium Digest, Vol. 3, 1992, pp. 1605-1608.

[3] M. D. Pocha, and R. L. Druce, "35 kV GaAs subnanosecond photoconductive switches," IEEE Trans. ED, vol.37, No.12, pp. 2473- 2492, Dec. 1990.

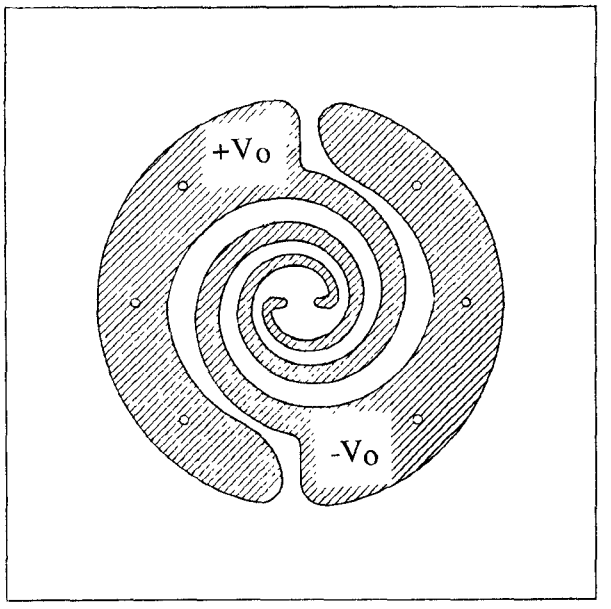

Fig.1 Top view of the monolithic, photoconductive ultra-wideband RF device with switching at center.

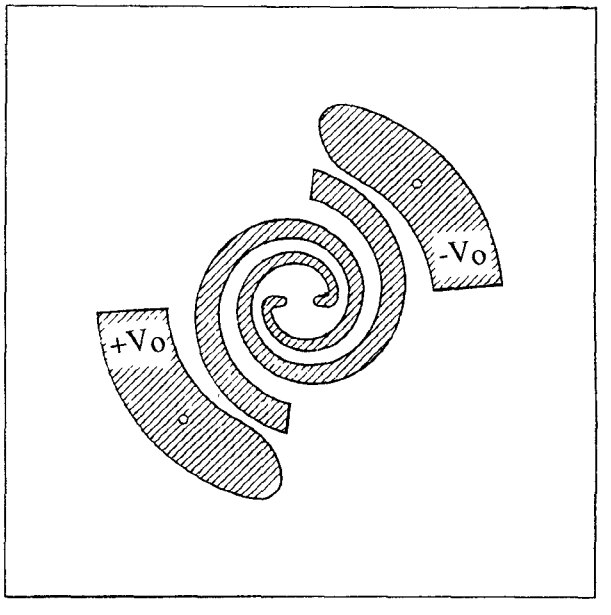

Fig.2 Top view of the monolithic, photoconductive ultra-wideband RF device with switching at edge.

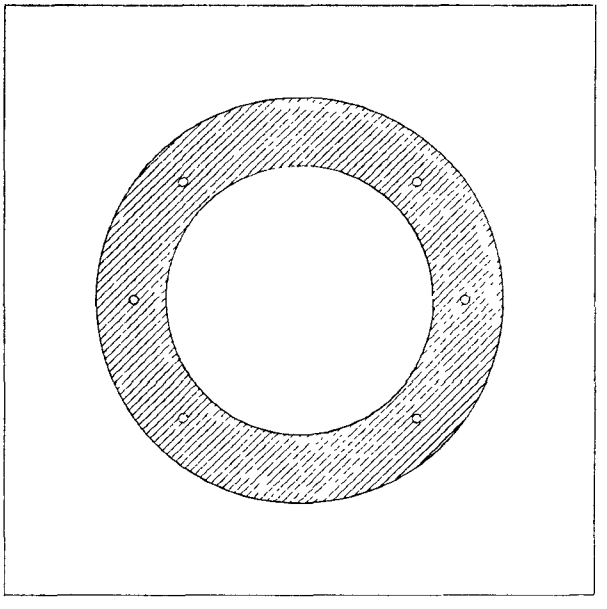

Fig.3 Bottom electrode of the monolithic, photoconductive ultra-wideband RF devices.

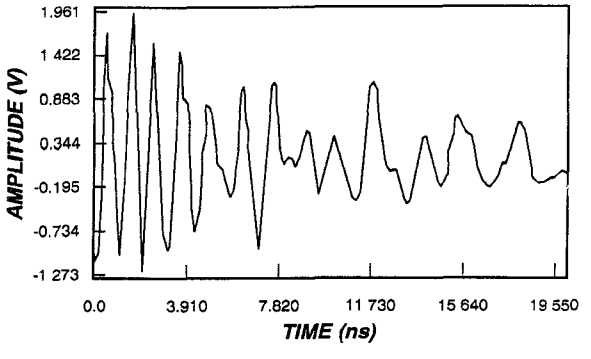

Fig.4 Output pulse obtained from the monolithic, photoconductive ultra-wideband RF device with switching at center.

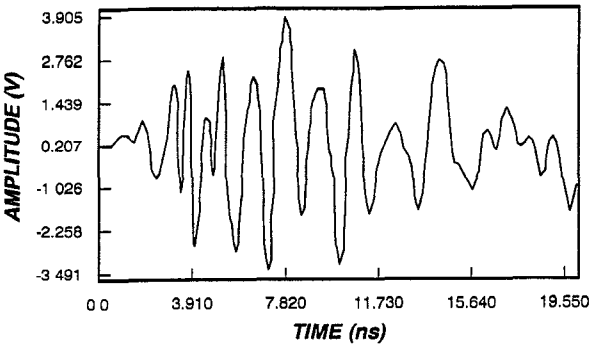

Fig.5 Output pulse obtained from the monolithic, photoconductive ultra-wideband RF device with switching at center.